Effects of grain size distribution on the packing fraction and shear strength of frictionless disk packings

Nicolas Estrada*

Departamento de Ingeniería Civil y Ambiental, Universidad de los Andes, Bogotá 111711, Colombia

(Received 28 July 2016; revised manuscript received 3 October 2016; published 16 December 2016)

Using discrete element methods, the effects of the grain size distribution on the density and the shear strength of frictionless disk packings are analyzed. Specifically, two recent findings on the relationship between the system's grain size distribution and its rheology are revisited, and their validity is tested across a broader range of distributions than what has been used in previous studies. First, the effects of the distribution on the solid fraction are explored. It is found that the distribution that produces the densest packing is not the uniform distribution by volume fractions as suggested in a recent publication. In fact, the maximal packing fraction is obtained when the grading curve follows a power law with an exponent close to 0.5 as suggested by Fuller and Thompson in 1907 and 1919 [Trans Am. Soc. Civ. Eng. **59**, 1 (1907) and *A Treatise on Concrete, Plain and Reinforced* (1919), respectively] while studying mixtures of cement and stone aggregates. Second, the effects of the distribution on the shear strength are analyzed. It is confirmed that these systems exhibit a small shear strength, even if composed of frictionless particles as has been shown recently in several works. It is also found that this shear strength is independent of the grain size distribution. This counterintuitive result has previously been shown for the uniform distribution by volume fractions. In this paper, it is shown that this observation keeps true for different shapes of the grain size distribution.

DOI: 10.1103/PhysRevE.94.062903

I. INTRODUCTION

Many granular materials, both natural and industrial, are composed of particles of different sizes. This fundamental property, commonly known as polydispersity, is of particular interest in various fields, such as geotechnical and process engineering, because it is known to have a strong effect on the material's macroscopic behavior. For example, polydispersity strongly influences the material's packing fraction, and, because of this, it is thought to have a major effect on the material's robustness. For this reason, choosing the correct grain size distribution (GSD) is an important step for proportioning the granular phase in composite materials, such as Portland concrete, asphalt concrete, and granular bases in roadway pavements in order to optimize their performance.

The relationship between polydispersity and the packing fraction has been studied for more than a century. Fuller and Thompson in 1907 [1] and 1919 [2] undertook the first experimental works in which they looked for the GSD of a mixture of cement and aggregates that produces the densest arrangement. This optimal GSD is important because it maximizes the concrete strength and workability. Fuller and Thompson found that the optimal GSD is that for which the cumulate volume distribution (also termed the grading curve in several industrial contexts) is that described by

$$\rho = (d/d_{\max})^{0.5}, \tag{1}$$

where ρ is the mass percentage of particles with diameters smaller than d and $d_{\max}$ is the maximal diameter. In the years that followed, similar experiments were conducted, such as those by Talbot and Richart [3] with cement and aggregates and those by Andreasen [4] with ceramic powders, and new exponents were proposed for Eq. (1) (i.e., 0.45 and 0.37, respectively). It was shown that the optimal exponent decreases as the amount of fines (i.e., particles smaller than 75 μm) in the mixture increases. Some recent experimental works are those reported in Refs. [5–8] in which different exponents are proposed, better adapted to different materials and industrial contexts. In addition, a correction to Eq. (1) was proposed [6], which takes into account a minimal diameter $d_{\min}$,

$$\rho = \left(\frac{d - d_{\min}}{d_{\max} - d_{\min}}\right)^{\eta}, \tag{2}$$

in which $d_{\max}$ and $d_{\min}$ determine the span of the GSD and the exponent η controls its shape (e.g., $\eta = 0$ corresponds to a monodisperse material, and $\eta = 1$ corresponds to the uniform distribution by volume fractions).

Other early works were those of Furnas in 1929 and 1931 [9,10] who was the first to develop analytical expressions to predict the packing density as a function of the GSD for both discrete and continuous GSDs. Other works in which similar expressions have been proposed are those reported in Refs. [11–21]. In general, these expressions yield better results for discrete GSDs (e.g., binary or ternary mixtures), especially when the difference between the diameters of each class is large. Predictions for continuous GSDs are less precise, probably due to the difficulty in understanding the interactions between particles of similar sizes.

A third strategy for tackling this problem theoretically consists of building arrangements of particles (usually disks or spheres) according to a geometrical rule and analyzing their structures. For example, different geometrical rules have allowed the empirical estimation of reference solid fractions, such as those of the random close packing [22–25] and the random loose packing [26] of equally sized disks (i.e., approximately 0.822 and 0.772, respectively). Some examples of works in which this strategy was used to study polydisperse systems are those reported in Refs. [17,27–36]. These models

*n.estrada22@uniandes.edu.co

constitute an analysis tool of great value since they allow for a large range of configurations to be explored with great computational efficiency. For example, the work of Voivret and colleagues [33] must be noted in which a large set of GSDs was built and compared. Different shapes of the GSDs were obtained by using the cumulative β distribution, finding that the GSD that produces the densest packing is the uniform distribution by volume fractions [i.e., Eq. (2) with $\eta = 1$]. This result disagrees with those reported in Refs. [1–3,5–8], although these works focus on mixtures of fine and coarse grains and the model developed in Ref. [33] was two dimensional.

The purpose of the tools mentioned in the previous paragraphs is to explore the relations between the GSD and the material's rheology and microstructure. However, the use of these tools implies several limitations. First, experiments are usually expensive and time consuming, especially if the researcher wants to explore a broad parametric space. Second, analytical predictions are difficult to extend in order to analyze properties beyond packing density, such as stiffness, shear strength, permeability, etc. In addition, the difficulty to study continuous GSDs constitutes a major obstacle for practical applications since most granular materials, both natural and industrial, exhibit continuous gradations. Finally, numerical models of arrangements built geometrically, which allow for investigating several microstructural characteristics, raise the question of the correspondence between these systems and real granular materials in which the system's behavior is the result of dynamics and of the interaction between grains.

A privileged analysis tool, which allows for overcoming most of these limitations, is numerical simulation using discrete element methods. However, the use of this tool also implies limitations, such as the need for a large number of grains in order to ensure statistical representativity and the need for a refined time discretization in order to correctly resolve the interactions between grains of very different sizes. In fact, these limitations, among others, could explain why most works using discrete element methods use narrow GSDs. In order to illustrate this statement, Fig. 1 shows the size ratio $\lambda = d_{\max}/d_{\min}$ that was used in all papers using discrete element simulations that have been published in the Granular Materials section of *Physical Review E* from 1 July 2015 to 1 July 2016. It is interesting to note that the mean $\langle\lambda\rangle$ is only 1.73 and that works using values of λ greater than 2 are rare, whereas natural granular materials, such as soils, usually have values of λ that are orders of magnitude larger.

Over the past decades, there have been a few research projects devoted to study the effects of the GSD by means of discrete element methods. Stroeven and Stroeven [37] presented simulations varying the shape of the GSD and found that this affects the packing density. Wackenhut and co-workers [38] compared the dilatancy and shear strength of a bidisperse material and one with a continuous GSD, finding that both measures were larger in the bidisperse material. Voivret and collegues [39] presented a systematic analysis of the anisotropy, force transmission, and shear strength in materials with continuous GSDs; they only varied the span of the GSD and kept its shape constant. An interesting and counterintuitive result of this paper is that the shear strength appears to be independent of the span of the GSD. Yohannes

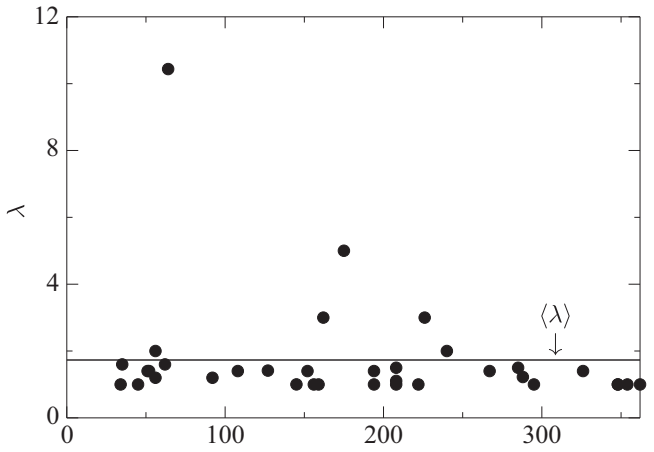

FIG. 1. Size ratio $\lambda = d_{\max}/d_{\min}$ used in all papers using discrete element simulations published in the Granular Materials section of *Physical Review E* from 1 July 2015 to 1 July 2016. The black line shows the average $\langle\lambda\rangle = 1.73$. The horizontal axis is the publication date, represented in days after 1 July 2015.

and Hill [40] studied the packing fraction and shear strength of bidisperse systems, highlighting how these measures depend on the level of inertia. Finally, the works of Nguyen and colleagues [41,42] must also be noted. They studied the effects of polydispersity on both particle size and particle shape, only varying the span of the GSD and finding that the shear strength was independent of the GSD as reported by Voivret *et al.* [39].

The works cited in the previous paragraph constitute valuable contributions to the study of polydisperse granular systems, and they evidence the great potential of simulations with discrete element methods to study the mechanical effects of polydispersity. However, these works also highlight the need for a systematic analysis that includes not only the span of the GSD, but also its shape. In addition, this bibliographic revision sheds light on two open questions for which the reported results disagree. These questions are the following:

(1) For coarse granular materials, is the GSD that produces the densest packing either that with $\eta \simeq 0.5$ as reported in Refs. [1,2] for three-dimensional (3D) experiments or that with $\eta = 1$ as reported in Ref. [33] for two-dimensional (2D) simulations?

(2) Is the shear strength constant not only with the span of the GSD as reported by Refs. [39,42], but also with the shape of the GSD?

The aim or this investigation was to explore these two questions. In order to do so, a discrete element method (i.e., contact dynamics) was used. The idea was to analyze the simplest possible systems for which the answer to these two questions was unclear. Thus, the particles were frictionless disks. The systems were mechanically densified, which allowed for studying their maximal packing fraction, and then sheared in a simple shear configuration, which allowed for studying their shear strength.

This article is organized as follows. First, the numerical method is briefly presented in Sec. II. In Sec. III, the methods used to construct the samples and to determine their maximal solid fraction and shear strength are described. The results are

presented in Sec. IV, and the paper ends in Sec. V with a brief conclusion and some perspectives.

II. NUMERICAL METHOD

The simulations were carried out using the contact dynamics method, developed in France by Moreau [43] and Jean in the 1990s [44–46]. This method can be seen as the combination of three main ingredients. The first ingredient is the set of equations of motion, which, integrated over a small time step, relate the impulsion to the change in momentum of each particle over the time step. The second ingredient is a set of contact laws, which relate the impulsions exerted at each contact with the change in relative velocity during the time step. The method supposes that grains are perfectly rigid, and the usual contact laws are perfect volume exclusion and Coulomb friction. The third ingredient of the method is an algorithm of solution. Since the system of equations to be solved is of implicit type, each grain's impulsions and changes in momentum are determined using an iterative algorithm similar to a Gauss-Seidel scheme. Then, these impulsions and changes in momentum are used to calculate the contact forces and grain positions at the end of the time step. For a detailed description of the contact dynamics method, see Refs. [47,48].

III. SIMULATIONS

A. Sample construction

The numerical samples were composed of approximately 10 000 disks with a GSD that followed a power law, such as that presented in Eq. (2). The span of the GSD was described by the size ratio $\lambda = d_{\max}/d_{\min}$, and the shape of the GSD was controlled by the exponent η. Systems were built for the following set of parameters: $\lambda \in (2,4,8,16,32)$ and $\eta \in (0.1,0.2,\ldots,1)$. For this purpose, the range of diameters $(d_{\min},d_{\max})$ was divided into ten subranges, and, inside these subranges, a uniform distribution by number of grains was used. Figure 2 shows the GSDs (i.e., the cumulate area distributions) of all samples; ρ is the area percentage of particles with a reduced diameter smaller than $d_r = (d - d_{\min})/(d_{\max} - d_{\min})$.

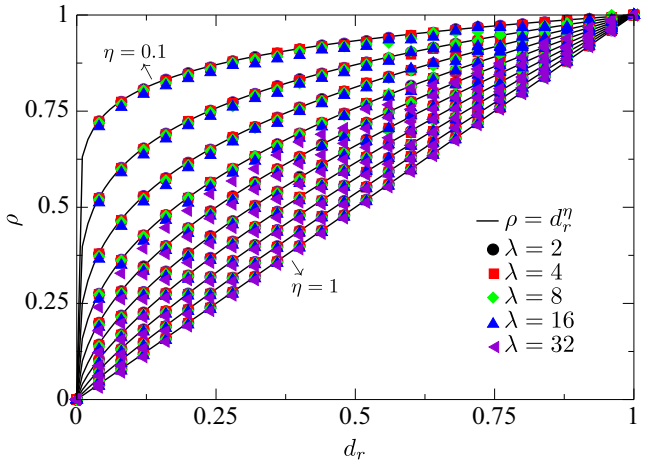

FIG. 2. Grain size distributions for all samples. The black lines show Eq. (2).

The black lines show Eq. (2). It can be seen that the built GSDs closely follow the theoretical curves. For $\lambda = 32$, only samples with $\eta \geq 0.4$ were built since it was seen that smaller values of η would require a larger number of grains in order to obtain a good fit (i.e., a maximal vertical offset of 0.03) with the theoretical curve.

B. Densification test

The samples were densified using an oedometric (i.e., zero lateral strain) compression test. For each of the samples, the grains initially were placed in the nodes of a square grid with n_r rows and n_c columns in which $n_r n_c \simeq 10\,000$. The length of the grid elements was $2.67\langle d\rangle$, where $\langle d\rangle = (d_{\max} + d_{\min})/2$ in order for the grains not to touch or overlap. Then, this arrangement of grains was placed inside a semiperiodic rectangular box (i.e., the top and bottom boundaries were rigid walls, and the lateral boundaries were periodic). Finally, a vertical force F was applied to the top and bottom walls, which induced the downward displacement of the top wall and the upward displacement of the bottom wall. The simulations stopped once the samples reached equilibrium. n_r and n_c varied among samples in order for the densified samples to be of approximately square shape. For each combination of parameters λ and η, five independent samples were built and densified. Figure 3 shows a schematic of the densification test.

Figure 4 shows a zoom of some of the samples after densification. In the first place, it can be seen that for low values of λ and η (i.e., for $\lambda = 2$ and/or $\eta = 0.1$) the packings are not completely random. This happens because for some GSDs most of the particles have almost the same size. As a result, some regions of the sample spontaneously arrange in an ordered fashion. Specifically, these "crystallized" regions emerge for GSDs with $\lambda = 2$ and/or $\eta \leqslant 0.3$. This implies that the construction-densification protocol presented in this paper cannot be used to reach reference states, such as the random close packing [22–25] and the random loose packing [26] of equally sized disks. In order to obtain these reference states, careful construction and analysis procedures must be implemented for ensuring the randomness of the system [22–26]. In the second place, it can be seen that for intermediate and large values of λ and η (i.e., for $\lambda \geqslant 4$ and $\eta \geqslant 0.4$) the packings are essentially disordered. In addition, visual

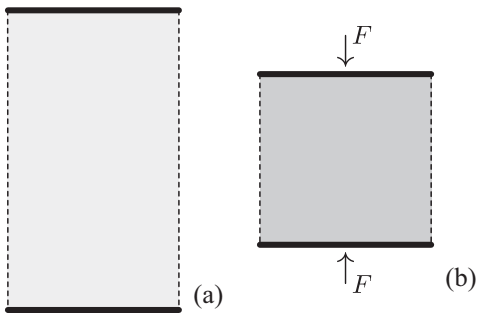

FIG. 3. Schematic of the densification test. The dashed lines represent periodic boundaries. (a) Initial state in which the grains neither touch nor overlap. (b) Final state once the sample reached equilibrium under the action of forces F.

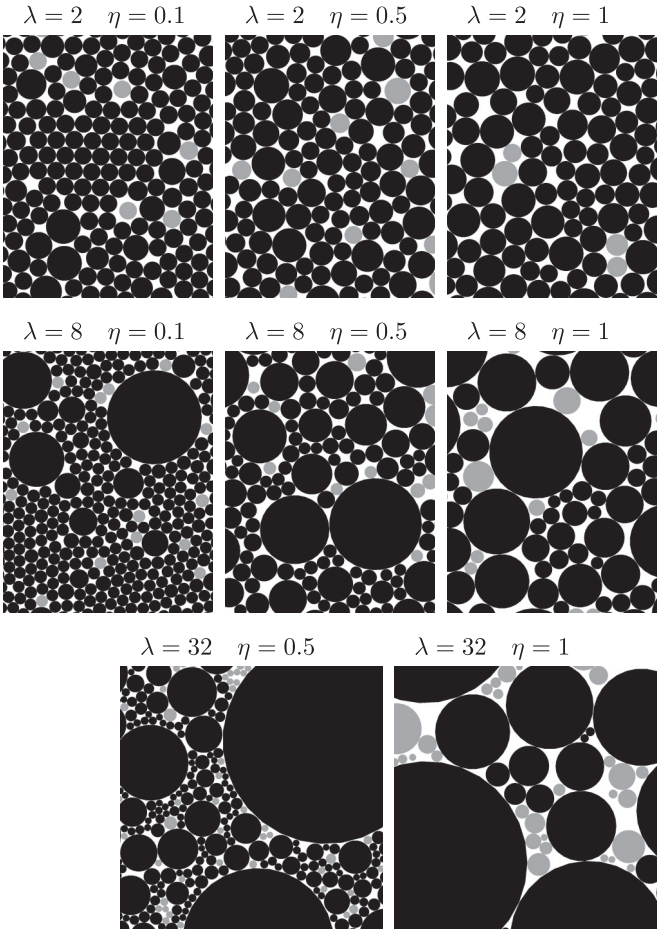

FIG. 4. Zoom of some of the samples at the end of the densification procedure. Floating particles (i.e., particles with one or no contacts) are shown in gray.

inspection of Fig. 4 reveals that the packings' density is strongly dependent on the choice of parameters λ and η. In particular, for $\eta = 0.5$ the small particles seem to better fill the pores between large particles, producing a denser system. This effect will be shown quantitatively in Sec. IV A.

C. Simple shear test

After densification, the samples were sheared by imposing a confining stress σ_c and a shear velocity v_s to the upper wall; see Fig. 5. In order to avoid strain localization along the boundaries, relative movement between the walls and the grains in contact with them was inhibited. For $\lambda \in (2,4,8,16)$, the samples were sheared to a shear strain $\gamma = \Delta x/h = 1$, where Δx is the horizontal displacement of the upper wall and h is the sample height. For $\lambda = 32$, γ was 0.5 because these simulations required considerable smaller time steps. It was verified that the shear strain was homogeneously distributed in the samples.

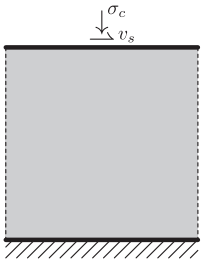

FIG. 5. Schematic of the shear test. The dashed lines represent periodic boundaries.

The level of inertia was quantified by means of the inertial number I [49], defined as

$$I = \frac{\dot{\gamma}\langle d\rangle}{\sqrt{\sigma_c/\varrho}}, \tag{3}$$

where $\dot{\gamma}$ is the shear rate and ϱ is the grains' density. In all shear tests $I \simeq 10^{-4}$, which means that these tests can reasonably be considered as quasistatic.

For all simulations, in both the densification and the simple shear tests, the gravity was set to zero.

IV. RESULTS

A. Packing fraction

The packing density was quantified by means of the packing fraction ν, defined as

$$\nu = \frac{A_g}{A}, \tag{4}$$

where A_g is the area occupied by the grains and A is the total area. Figure 6 shows ν as a function of η for all values of λ. First, it can be seen that ν increases with λ as expected and as shown previously in Refs. [39,42]. Second, it can be seen that ν varies in a nonmonotonic fashion with η with a maximum for $\eta \simeq 0.5$. This shows that the maximal packing fraction is obtained when the GSD follows a power law with an exponent

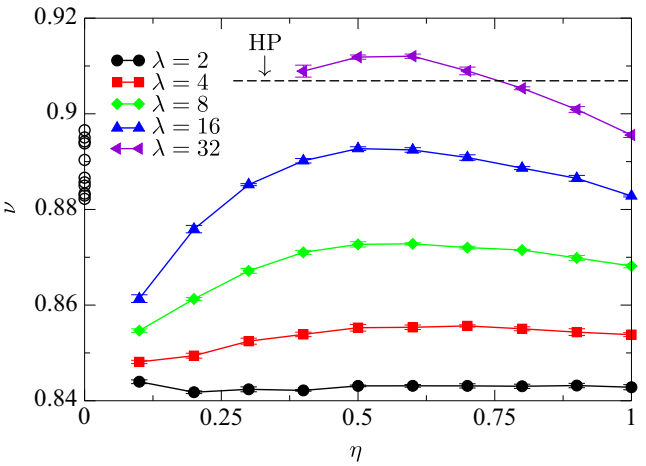

FIG. 6. Packing fraction ν as a function of η for all values of λ. Error bars indicate the standard deviation between the five realizations of the densification test for each combination of parameters λ and η. The empty circles on the left axis show ν for several equally sized disk packings, built following the protocol described in Sec. III B (the difference between these systems is the remainder of the box width divided by the disks' diameter, which controls the amount and extent of dislocations). The dashed line indicates the packing fraction of a set of disks of the same size packed in an hexagonal arrangement HP [i.e., $\pi/(2\sqrt{3}) \approx 0.9069$].

close to 0.5 as suggested by Fuller and Thompson [1] and Taylor and Thompson [2] and not for the uniform distribution by volume fractions (i.e., for $\eta = 1$), as suggested by Voivret *et al.* [33]. As shown qualitatively in Fig. 4, large packing fractions can be obtained by combining three key features: disorder, a large size span, and the correct proportion of small particles that allows for the voids between the large particles to be efficiently filled.

Moreover, Fig. 6 also shows that ν can exceed the packing fraction of a set of equally sized disks, which spontaneously arrange in a crystallized fashion. The empty circles on the left axis show ν for several equally sized disk packings, built following the protocol described in Sec. III B (the difference between these systems is the remainder of the box width divided by the disks' diameter, which controls the amount and extent of dislocations). The dashed line shows ν for the hexagonal arrangement [i.e., $\pi/(2\sqrt{3}) \approx 0.9069$], which is the highest covering density that can be achieved with equally sized disks.

B. Shear strength

In order to calculate the shear strength, it is useful to calculate the stress tensor. To do so, we first compute the internal moment tensor $\boldsymbol{M}^g$ of each grain g, defined as

$$M_{ij}^g = \sum_{c \in g} f_i^c r_j^c, \tag{5}$$

where i and j represent the components in an orthonormal reference frame, $\boldsymbol{f}^c$ is the force exerted on the grain at contact c, $\boldsymbol{r}^c$ is the position vector of the same contact, and the sum runs over all contacts on the grain. The stress tensor $\boldsymbol{\sigma}$ in an area A of the granular assembly is given by

$$\sigma_{ij}^A = \frac{1}{A} \sum_{g \in A} M_{ij}^g. \tag{6}$$

The shear strength can then be quantified by the angle of internal friction ϕ, which can be calculated as

$$\phi = \arctan \frac{\sigma_{xy}}{\sigma_{yy}}, \tag{7}$$

where x and y represent, respectively, the horizontal and vertical directions in Fig. 5.

As examples, Fig. 7 shows ϕ and ν as functions of the shear strain γ for five samples. First, it can be seen that both ϕ and ν fluctuate around a mean value, indicating that the packing is being sheared in the steady state. Second, it can be seen that the shear strength is similar in the five samples and is close to 6°. This means that these packings exhibit a small shear strength even if they are composed by frictionless grains. Finally, it can be seen that ν remains approximately constant during the test. These two last observations confirm that, as first shown by Peyneau and Roux, "Frictionless bead packs have macroscopic friction, but no dilatancy" [50] and Azéma *et al.* [51].

Figure 8 shows ϕ as a function of η for all values of λ. It can be seen that ϕ remains constant for both λ and η. First, this means that, as shown in Refs. [39,42], the shear strength is independent of the span of the GSD. Second, this means that the shear strength is also independent of the shape of the GSD, at least for the family of shapes that can be described by Eq. (2).

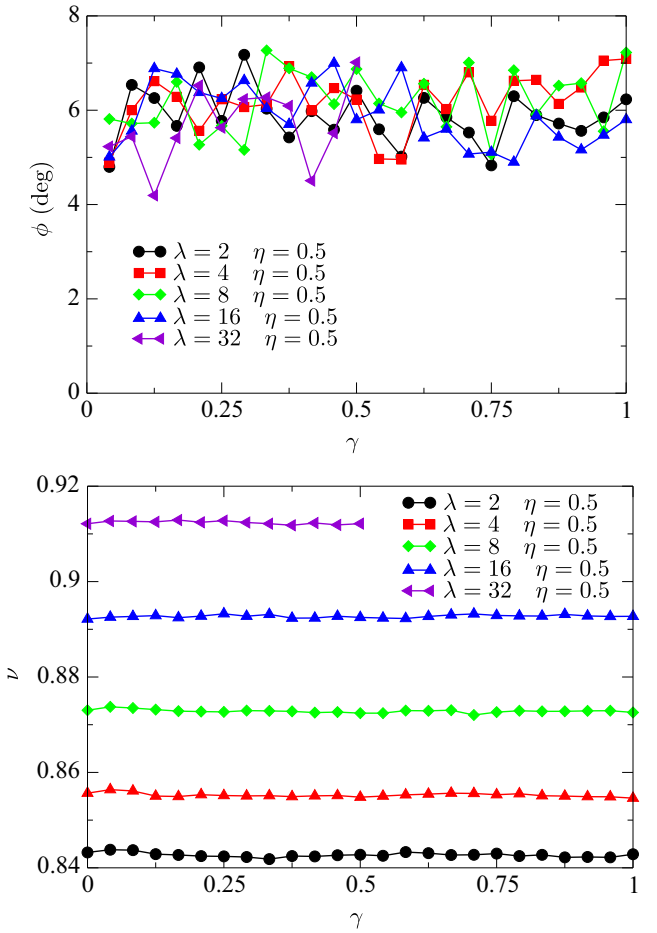

FIG. 7. Angle of internal friction ϕ (top) and packing fraction ν (bottom) as functions of the shear strain γ for five samples.

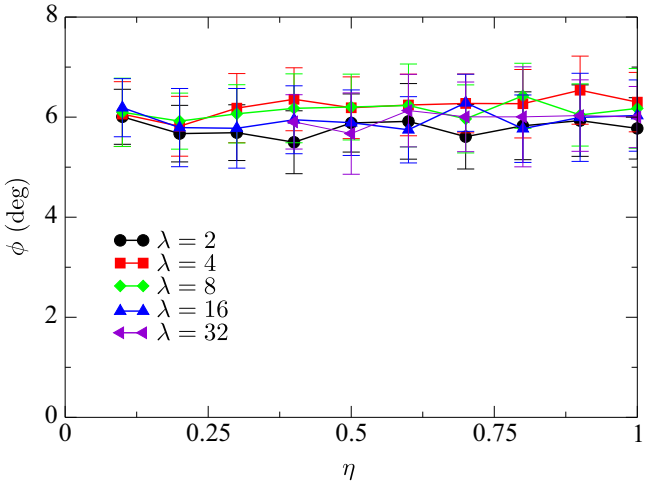

FIG. 8. Shear strength ϕ as a function of η for all values of λ. Error bars indicate the standard deviation of 25 different states captured during the shear tests.

V. CONCLUSION AND PERSPECTIVES

The purpose of this paper was to explore the following two questions for which the reported results disagree:

(1) For coarse granular materials, is the GSD that produces the densest packing either that described by a power law with an exponent close to 0.5 as reported in Refs. [1,2] for 3D experiments or the uniform distribution by volume fraction as reported in Ref. [33] for 2D simulations?

(2) Is the shear strength constant not only with the span of the GSD as reported by Refs. [39,42], but also with the shape of the GSD?

Regarding the first question, it was shown that the maximal packing fraction is obtained when the GSD follows a power law with an exponent close to 0.5 as suggested by Fuller and Thompson in 1907 [1] and Taylor and Thompson in 1919 [2] and not for the uniform distribution by volume fractions (i.e., for an exponent equal to 1) as suggested recently by Voivret *et al.* [33]. This result extends the validity of the optimal GSD proposed in Refs. [1,2] for real granular materials to the case of 2D frictionless disks. Moreover, based on a qualitative observation, it was suggested that the high packing fraction of the GSD proposed by Fuller and Thompson is due to a higher proportion of small particles that allows for the voids between the large particles to be efficiently filled. Evidently, the effect is enhanced as the span of the GSD increases.

When comparing the results presented in the present paper with those presented in Ref. [33], it must be noted that the parametric space investigated in Ref. [33] did not include a power law GSD with an exponent of 0.5. In addition it is also of importance that the numerical protocol used by Voivret and colleagues to build the samples is different from the one used in the present paper since that used in Ref. [33] is based on geometrical rules and that used here is of a mechanical nature.

Regarding the second question, it was shown that the shear strength remains constant for both the span (i.e., λ) and the shape (i.e., η) of the GSD. This result is in agreement with that presented by Voivret *et al.* [39] and Nguyen *et al.* [42] and shows that it can be generalized to the family of shapes described by Eq. (2). Finally, our results confirm that systems composed of frictionless particles have a small shear strength but no dilatancy as was first shown by Peyneau and Roux [50] and Azéma *et al.* [51].

This work will be continued in several directions. First, the effects of the GSD in the system's microstructure will be analyzed in both static loading and quasistatic shear conditions. Second, the effects of the GSD on the packing fraction and the shear strength of three-dimensional systems will be explored. This is a crucial task in line with applying the results of discrete element simulations to real systems and industrial processes.

ACKNOWLEDGMENTS

The author thanks C. M. Gutiérrez for her helpful advice and stimulating discussions. Also thanked are J. P. Carmona and J. M. Torres for their help with numerical simulations.

[1] W. B. Fuller and S. E. Thompson, Trans. Am. Soc. Civ. Eng. **59**, 1 (1907).
[2] F. W. Taylor and S. E. Thompson, *A Treatise on Concrete, Plain and Reinforced* (Wiley, New York, 1919).
[3] A. N. Talbot and F. E. Richart, Bull.-Illinois, Univ., Eng. Exp. Stn. **21**, 1 (1923).
[4] A. H. M. Andreasen, Kolloid-Zeitschrift **50**, 217 (1930).
[5] J. M. S. Shilstone, Concr. Int.: Des. Constr. **12**, 33 (1990).
[6] J. E. Funk and D. R. Dinger, *Predictive Process Control of Crowded Particulate Suspension* (Springer, New York, 1994).
[7] P. N. Quiroga and D. W. Fowler, ICAR Technical Reports, 2004 (unpublished).
[8] H. J. H. Brouwers and H. J. Radix, Cem. Concr. Res. **35**, 2116 (2005).
[9] C. C. Furnas, Bulletin of US Bureau of Mines **307**, 74 (1929).
[10] C. C. Furnas, Ind. Eng. Chem. **23**, 1052 (1931).
[11] R. F. Fedors and R. F. Landel, Powder Technol. **23**, 225 (1979).
[12] N. Ouchiyama and T. Tanaka, Ind. Eng. Chem. **23**, 490 (1984).
[13] N. Ouchiyama and T. Tanaka, Ind. Eng. Chem. Fundam. **25**, 125 (1986).
[14] T. Stovall, F. de Larrard, and M. Buil, Powder Technol. **48**, 1 (1986).
[15] A. B. Yu and N. Standish, Powder Technol. **55**, 171 (1988).
[16] A. B. Yu and N. Standish, Powder Technol. **76**, 113 (1993).
[17] T. Aste, Phys. Rev. E **53**, 2571 (1996).
[18] H. J. H. Brouwers, Phys. Rev. E **74**, 031309 (2006).
[19] H. J. H. Brouwers, Phys. Rev. E **84**, 042301 (2011).
[20] H. J. H. Brouwers, Phys. Rev. E **87**, 032202 (2013).
[21] H. J. H. Brouwers, Phys. Rev. E **89**, 052211 (2014).
[22] H. H. Kausch, D. G. Fesko, and N. W. Tschoegl, J. Colloid Interface Sci. **37**, 603 (1971).
[23] T. I. Quickenden and G. K. Tan, J. Colloid Interface Sci. **48**, 382 (1974).
[24] D. N. Sutherland, J. Colloid Interface Sci. **60**, 96 (1977).
[25] J. G. Berryman, Phys. Rev. A **27**, 1053 (1983).
[26] E. L. Hinrichsen, J. Feder, and T. Jossang, Phys. Rev. A **41**, 4199 (1990).
[27] A. Bezrukov, D. Stoyan, and M. Bargiel, Image Anal. Stereol. **20**, 203 (2001).
[28] P. S. Dodds and J. S. Weitz, Phys. Rev. E **65**, 056108 (2002).
[29] M. Wackenhut and H. Herrmann, Phys. Rev. E **68**, 041303 (2003).
[30] H. J. Herrmann, R. Mahmoodi Baram, and M. Wackenhut, Physica A **330**, 77 (2003).
[31] K. Sobolev and A. Amirjanov, Adv. Powder Technol. **15**, 365 (2004).
[32] K. Sobolev and A. Amirjanov, Powder Technol. **141**, 155 (2004).
[33] C. Voivret, F. Radjaï, J.-Y. Delenne, and M. S. El Youssoufi, Phys. Rev. E **76**, 021301 (2007).
[34] J.-F. Jerier, V. Richefeu, D. Imbault, and F.-V. Donzé, Comput. Methods Appl. Mech. Eng. **199**, 1668 (2010).
[35] K. Sobolev and A. Amirjanov, Constr. Building Mater. **24**, 1449 (2010).

[36] S. D. S. Reis, N. A. M. Araújo, J. S. Andrade, Jr., and H. J. Herrmann, Europhys. Lett. **97**, 18004 (2012).
[37] P. Stroeven and M. Stroeven, Cement Concr. Res. **29**, 1201 (1999).
[38] M. Wackenhut, S. McNamara, and H. Herrmann, Eur. Phys. J. E **17**, 237 (2005).
[39] C. Voivret, F. Radjaï, J.-Y. Delenne, and M. S. El Youssoufi, Phys. Rev. Lett. **102**, 178001 (2009).
[40] B. Yohannes and K. M. Hill, Chaos **82**, 061301 (2010).
[41] D.-H. Nguyen, E. Azéma, F. Radjaï, and P. Sornay, Phys. Rev. E **90**, 012202 (2014).
[42] D.-H. Nguyen, E. Azéma, P. Sornay, and F. Radjaï, Phys. Rev. E **91**, 032203 (2015).
[43] J. J. Moreau, Eur. J. Mech. A. Solids **13**, 93 (1994).
[44] M. Jean, *Mechanics of Geometrical Interfaces* (Elsevier, New York, 1995), pp. 463–486.
[45] M. Jean, Comput. Methods Appl. Mech. Eng. **177**, 235 (1999).
[46] M. Jean, *Micromécanique des Matériaux Granulaires* (Hermes, Paris, 2001), pp. 199–324.
[47] F. Radjai and V. Richefeu, Mech. Mater. **41**, 715 (2009).
[48] *Discrete Numerical Modeling of Granular Materials*, edited by F. Radjai and F. Dubois (Wiley-ISTE, New York, 2011).
[49] GDR-MiDi, Eur. Phys. J. E **14**, 341 (2004).
[50] P.-E. Peyneau and J.-N. Roux, Phys. Rev. E **78**, 011307 (2008).
[51] E. Azéma, F. Radjai, and J.-N. Roux, Phys. Rev. E **91**, 010202 (2015).